Catalysis Science & Technology

Accepted Manuscript

ROYAL SOCIETY OF CHEMISTRY

www.rsc.org/catalysis

Specific oriented recognition of a new stable ICTX@Mfa with retrievability for selectively photocatalytic degrading ciprofloxacin

Ziyang Lu,[a,b] Zhi Zhu,[b] Dandan Wang,[b] Zhongfei Ma,[a] Weidong Shi,[b] Yongsheng Yan,[*,b] Xiaoxu Zhao,[b] Hongjun Dong,[*,b] Li Yang,[b] Zhoufa Hua,[b]

(a. School of the Environment and Safety Engineering, Jiangsu University, Jiangsu, Zhenjiang 212013, PR China b. School of Chemistry & Chemical Engineering, Jiangsu University, Jiangsu, Zhenjiang 212013, PR China)

Abstract

A new imprinted photocatalyst ICTX@Mfa is prepared by employing the molecular imprinting technique, which is authenticated via a variety of modern analysis methods. It exhibits the superior specific oriented recognition capability, stability and retrievability for selectively degrading common antibiotic ciprofloxacin molecules under the visible light. Through getting insight into the photocatalytic mechanism of ciprofloxacin molecules over ICTX@Mfa, we can confirm that the generation of holes and hydroxyl radicals plays a major role in degrading ciprofloxacin in virtue of the active species detection experiments. This work puts forward a new design idea and provides an illustrative example for selectively oriented removing the specified organic pollutant molecules according to the practical requirements.

Keywords: ICTX@Mfa; Imprinted photocatalyst; Selectivity; Retrievability; Degradation mechanism

* Corresponding author. Tel.: +86 511 88791800; Fax: +86 511 88791800.
E-mail address: luziyang126@126.com (Y.S. Yan), donghongjun6698@aliyun.com (H.J. Dong).

Introduction

The environmental pollution that is getting more and more serious has already threatened the survival and development of human and other organisms[1]. Using a new generation of green environmental protection technology to solve the problems of water and air environmental pollution has become an arduous challenge. In recent years, the solar photocatalytic approach has been aroused widespread attention and investigation, which is consistently identified as a more promising candidate to remedy or even replace the traditional advanced oxidation technologies such as chemical, biological and physical methods[1-5]. Therefore the exploitation of novel, high-efficient and eco-friendly photocatalytic materials has been a primary issue so that it can be actually applied to air purification and wastewater cleaning by making full use of solar energy[6-9].

At present, Ti-based compounds have attached great interest in the organic contaminant treatment fields due to its good performance such as low-cost, non-toxicity, good chemical and thermal stability etc[10, 11]. For instance, TiO_2 is one of the earliest research and most promising photocatalytic materials[12, 13]. Nevertheless, some inherent defects of TiO_2 have limited its practical application, such as the relative wide band gap (~3.2 eV) which cannot respond to visible light, low recovery rate which is difficult to recycling utilization and low selectivity which is short of oriented recognition ability[14-20]. Because the molecular imprinting technique is a conveniently powerful method for preparing imprinted polymer with the recognition ability by binding the template molecules[21-27], some literatures report that the polymer layer with the imprinted cavity is coated on the surface TiO_2 to realize selective photodegradation. However, it usually covers active sites of TiO_2 and reduces contact area between target molecules and photocatalyst, leading to the

distinct decrease of photocatalytic activity[28, 29]. Although some researches attempt to directly imprint on the surface of TiO_2 using organic/inorganic template molecules/ions, it is usually wanting in specific oriented recognition ability[30-37]. At the same time, the high-temperature calcination may cause the collapse of imprinted cavities and further decrease the selectivity.

Therefore, exploiting the novel, high-efficient and recoverable Ti-based photocatalyst with the superior visible light response and selectivity has the important theoretical research significance and potential application value. In practice, most researchers pursue, all the while, the regulate and control of TiO_2 including its mico/nano-structure, morphology, and composite etc, but neglecting that $Ti(OH)_4$ precursor produced usually in its preparation. $Ti(OH)_4$ xerogel is also relative stable semiconductor and obtained expediently by the hydrolysis reaction of titanates (e.g. tetrabutyl titanate). In the meantime, it is also very easy to shape and mold without calcination, which is applied to serving as one candidate to prepare imprinted photocatalytic materials. Furthermore, taking account of the visible light harvest ability, cost consumption and retrievability, Co^{2+} and magnetic fly-ash (Mfa) are introduced into $Ti(OH)_4$ photocatalyst system to act as a dopant and supporter, respectively. One hand, Co^{2+} dopant usually can widen a visible light absorption of semiconductor and even produce trailing and extend to near infrared region, which has most researches to be applied to enhancing photocatalytic activity of photocatalysts[38-41]. On the other hand, Mfa, composed mainly of Fe_2O_3, SiO_2 and Al_2O_3, etc., can be screened out from the coal fly ash in solid wastes generated from the combustion of coal[42]. It has been widely used as a promising supporter[43-45] and carrier[46-48] to realize the waste utilization owing to its favorable properties of the high chemical stability, low cost, uniform spherical morphology and magnetic property and so on.

Therefore, in this work, the Co^{2+} ions doped $Ti(OH)_4$ xerogel supported by Mfa (ICTX@Mfa) as a new imprinted photocatalyst is prepared by the molecular imprinting technique. Using common antibiotic ciprofloxacin as a template molecule specimen, ICTX@Mfa not only has the high specific oriented recognition capability for selectively degrading ciprofloxacin under the visible light, but also exhibits superior stability and retrievability. Besides, the photocatalytic degradation mechanism of ciprofloxacin is also discussed.

Experimental

Preparation

Ciprofloxacin, danofloxacin mesylate and tetracycline were purchased from National Institutes for Food and Drug Control. Cobalt chloride hexahydrate ($CoCl_2 \cdot 6H_2O$, A.R.), 3-aminopropyltriethoxysilane (A.R.), N, N-dimethylformamide (A.R.) and succinic anhydride (A.R.) were supported by Aladdin Chemistry Co., Ltd. Tetrabutyl titanate (C.R.), toluene (A.R.), methanol (A.R.), anhydrous ethanol (A.R.) and hydrochloric acid (HCl, 37.8%) were all purchased from Sinopharm Chemical Reagent Co., Ltd. Coal fly ash was friendly supported by China Power Yaomeng Power Co., Ltd. Nitrogen was supported from INHONG GAS. Deionized water was used throughout this work.

Magnetic fly-ash (Mfa) was isolated from coal fly ash by a magnet and screened out between 75 μm and 86 μm. Afterwards, the Mfa was modified according to our previous work[28]. Firstly, Mfa of 6 g was added into hydrochloric acid of 100 mL with 1 mol L^{-1} under mechanical agitation for 3 h at 353 K, and then washed with deionized water and dried at 323 K. Secondly, above acid-activated Mfa of 3 g and 3-aminopropyltriethoxysilane of 8 mL were added into toluene of 100 mL under mechanical agitation for 12 h at 343 K in the nitrogen atmosphere, and then filtered

by toluene and methanol. Lastly, above product of 3 g was added into N, N-dimethylformamide of 40 mL containing succinic anhydride (0.5 mol L^{-1}) under mechanical agitation for 24 h at 303 K, and then washed with N, N-dimethylformamide and dried at 323 K, the modified Mfa was obtained.

The non-imprinted $Ti(OH)_4$ xerogel@Mfa (NITX@Mfa) was prepared as follows. Tetrabutyl titanate of 6 mL was added into anhydrous ethanol of 35 mL under mechanical agitation for 30 min at 313 K. Afterwards, the mixed solution of anhydrous ethanol (35 mL), deionized water (3 mL) and hydrochloric acid (0.2 mL) were added into above mixture drop by drop. When the sol began to form, the modified Mfa of 1 g was added into above sol and kept stirring until the gel was generated. After the gel was dried at 323 K, NITX@Mfa was obtained.

The imprinted $Ti(OH)_4$ xerogel@Mfa (ITX@Mfa) was prepared as follows. Firstly, tetrabutyl titanate of 6 mL was added into 35 mL anhydrous ethanol under mechanical agitation for 30 min at 313 K. Afterwards, ciprofloxacin of 0.01 mol was added into above solution under mechanical agitation for another 10 min at 313 K. Secondly, the mixed solution of anhydrous ethanol (35 mL), deionized water (3 mL) and hydrochloric acid (0.2 mL) were added into above mixture drop by drop. When the sol began to form, the modified Mfa of 1 g was added into above sol and kept stirring until the gel was generated. Thirdly, after the gel was dried at 323 K, the obtained xerogel was added into 200 mL deionized water and exposed to a 500 W tungsten lamp (the illumination of tungsten lamp could reach 9.5×10^4 lux) for 3 h under magnetic agitation in the air to remove ciprofloxacin (template molecule). Finally, after the product was washed with deionized water and anhydrous ethanol in turn and dried at 323 K, ITX@Mfa was obtained. The preparation of imprinted Co^{2+} doped $Ti(OH)_4$ xerogel@Mfa (ICTX@Mfa) is similar to that of ITX@Mfa. When

ciprofloxacin of 0.01 mol and $CoCl_2 \cdot 6H_2O$ of 0.0015 mol were added simultaneously, ICTX@Mfa was obtained. Meanwhile, the non-imprinted Co^{2+} doped $Ti(OH)_4$ xerogel@Mfa (NICTX@Mfa) was obtained except adding ciprofloxacin and the visible light irradiation in the preparation of ICTX@Mfa.

Characterization

XRD patterns were obtained with a D8 ADVANCE X-ray diffractometer (Bruker AXS Co., Germany). Inductively coupled plasma optical emission spectrometry (ICP-OES, VISTA-MPX) was designed to analyze mental contents of the samples by heating acid digestion method. The sample preparation is that the product (0.05 g) was dissolved with HNO_3 (4 mL), HF (8 mL) and HCl (8 mL) and diluted to 250 mL with distilled water. Fourier-transformed infrared (FT-IR) spectra of the samples were recorded on a Nicolet Nexus 470 FT-IR (Thermo Nicolet Co., USA) with 2.0 cm^{-1} resolution in the range 400 cm^{-1} - 4000 cm^{-1}, using KBr pellets. A Vario EL elemental analyzer (Elementar, Hanau, Germany) was employed to investigate the surface nonmetal contents of the prepared samples. The morphology was observed by a scanning electron microscopy (SEM, S-4800). The specific surface area, pore volume and average pore diameter of the samples were measured by using a NOVA 2000e analytical system (Quantachrome Co., USA). UV-vis diffused reflectance spectra (UV-vis DRS) were obtained for the dry-pressed disk samples using 2450 spectrometer (Shimazu Co., Japan) equipped with the integrated sphere accessory for diffused reflectance spectra, using $BaSO_4$ as the reflectance sample. Magnetic measurement was carried out using a vibrating sample magnetometer (VSM) (7300, Lakeshore) under a magnetic field up to 10 kOe. X−ray photoelectron spectroscopy (XPS) was measured with a PHI5300 spectrometer using Al K (12.5 kV) X−ray source.

Adsorption property

The adsorption capacity was tested in accordance with the following steps: The sample of 0.1 g was added into ciprofloxacin solution of 10 mg L^{-1} (100 mL), and analyzed at interval of 5 min at 303 K. After 40 min in the dark, the sample was isolated by a magnet, and the concentration of solution was measured with the UV-vis spectrophotometer 2450 (Shimazu Co., Japan). Three repeated experiments were adopted to ensure the reliability of the experimental data.

Photodegradation activity

The photocatalytic reaction was conducted in a photocatalytic reactor at 303 K under the visible light irradiation provided by the 500 W tungsten lamp with the illumination of 9.5×10^4 lux. The photocatalytic reaction flask contained sample of 0.1 g and ciprofloxacin solution of 10 mg L^{-1} (100 mL) (or danofloxacin mesylate of 20 mg L^{-1} or tetracycline of 20 mg L^{-1}). After the desired time in the dark, the initial concentration was determined. Afterwards, the concentration was measured with the UV-vis spectrophotometer 2450 at interval of 20 min accompanied by aeration rate of 2 mL min^{-1}. Three repeated experiments were adopted to ensure the reliability of the experimental data. The degradation rate (Dr.) was calculated by using the following formula. C_0 and C are the initial concentration and reaction concentration of antibiotic solution, respectively.

$$\mathrm{Dr.} = \left(1 - \frac{C}{C_0}\right) \times 100\%$$

The circle experiments were further performed as follows. After first reaction, the sample was isolated by a magnet and sonicated with anhydrous ethanol for 0.5 h to remove the residual ciprofloxacin and by-products. After the product was washed with deionized water and dried, it was performed the next photodegradation reaction. This procedure was repeated five times to

confirm the stability of the samples. Three repeated experiments were adopted to ensure the reliability of the experimental data.

Results and discussion

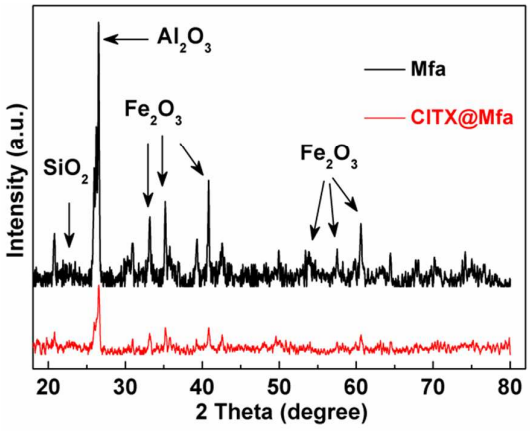

Fig. 1 XRD patterns of Mfa and ICTX@Mfa

The target product of imprinted Co^{2+} doped $Ti(OH)_4$ xerogel@Mfa (ICTX@Mfa) is firstly investigated by XRD with the help of comparing with Mfa. As shown in Fig. 1a, some diffraction peaks are observed in the diffraction pattern of Mfa, which are assigned to Fe_2O_3, SiO_2 and Al_2O_3 etc. major constituents in Mfa and agree well with the results of our previous reports[23]. The diffraction peaks belonging to $Ti(OH)_4$ xerogel are not observed, which may be attributed to the reason that it has the relatively low crystallinity and its diffraction signals can also be covered by the diffraction peaks of Mfa. Furthermore, the diffraction peak intensities of ICTX@Mfa become weaker compared with that of Mfa, which indirectly indicates that the imprinted Co^{2+} doped $Ti(OH)_4$ xerogel layer is coated on the surface of Mfa.

Table 1 Metal contents of Mfa, NITX@Mfa , ITX@Mfa , NICTX@Mfa and ICTX@Mfa

Samples	Fe (%)	Si (%)	Al (%)	Ti (%)	Co (%)
Mfa	13.83	13.59	7.47	0	0
NITX@Mfa	8.02	7.96	4.11	16.73	0

ITX@Mfa	7.95	7.89	4.02	16.46	0
NICTX@Mfa	7.98	7.94	4.09	16.27	1.54
ICTX@Mfa	7.99	7.92	4.08	15.71	1.38

Moreover, in order to further verify the formation of ICTX@Mfa and other as-prepared samples, the mental contents of Mfa, non-imprinted NITX@Mfa, imprinted ITX@Mfa, non-imprinted NICTX@Mfa and imprinted ICTX@Mfa are analyzed by ICP-OES. From the Table 1, Mfa mainly contains Fe (13.83%), Si (13.59%) and Al (7.47%) without Ti and Co elements. When the surface of Mfa is modified by $Ti(OH)_4$ xerogel layer, the Ti contents of 16.73 % and 16.46 % are detected in the NITX@Mfa and ITX@Mfa samples, respectively. Meanwhile, when Co^{2+} doping experiments are performed, Co element is also detected besides Ti element, the content of that is 1.54% and 1.38% in the NICTX@Mfa and ICTX@Mfa samples, respectively. It demonstrates that Co^{2+} doped $Ti(OH)_4$ xerogel layer is successfully coated on the surface of Mfa.

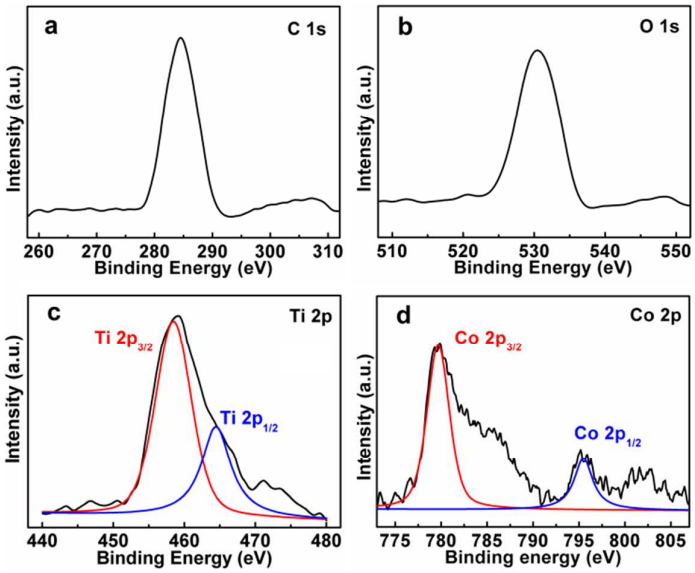

Fig. 2 XPS spectra of ICTX@Mfa

In addition, the XPS spectra of the ICTX@Mfa sample are investigated to clarify the valance

state of each element on the surface. Fig. 2a describes the C^{4+} 1s spectrum, which origins from carbon pollutions absorbed on the surface of ICTX@Mfa. The peak at 530.6 eV binding energy in Fig 2b derives from O^{2-} 1s state of the $Ti(OH)_4$ xerogel layer. In addition, Fig. 2c displays the obvious emission peak of Ti 2p state. After separating peak, the peaks located at 464.5 eV and 458.5 eV binding energies are consistent with the feature peak of Ti^{4+} $2p_{1/2}$ and Ti^{4+} $2p_{3/2}$ states[49]. Moreover, the XPS spectrum of Co^{2+} 2p state shown in Fig. 2d consists of two individual peaks centered at 779.7 eV and 795.5 eV, which are ascribed to the emissions of Co^{2+} $3p_{3/2}$ and Co^{2+} $3p_{1/2}$ states binding energies, respectively[49]. The above results further indicate that the Co^{2+} ions doped $Ti(OH)_4$ xerogel layer is coated on the surface of Mfa.

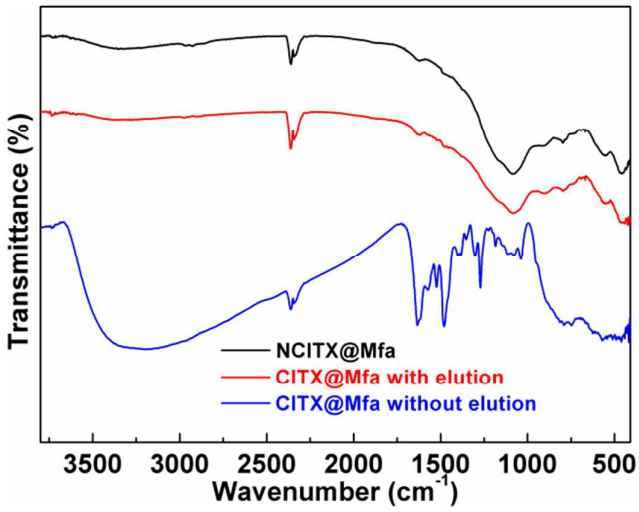

Fig. 3 FT-IR spectra of NICTX@Mfa, ICTX@Mfa with elution and ICTX@Mfa without elution

For the purpose of testifying that ciprofloxacin molecules can embed in and dislodge from the external $Ti(OH)_4$ xerogel layer, the FT-IR spectra of non-imprinted NICTX@Mfa, imprinted ICTX@Mfa with elution, and imprinted ICTX@Mfa without elution are recorded in the range of 4000 cm^{-1} to 400 cm^{-1}. As given in Fig. 3, we find that the spectrum of imprinted ICTX@Mfa with elution sample is similar to that of non-imprinted NICTX@Mfa, which fully indicates that ciprofloxacin molecules have been almost washed off. The absorption band at 3400 cm^{-1} and 1100

cm^{-1} are assigned to the stretching of hydroxyl groups (-OH) and asymmetric stretching of silica-oxygen (Si-O) single bonds, respectively[28]. The absorption bands from 600 cm^{-1} to 400 cm^{-1} are attributed to the inorganic oxide absorption bands in Mfa[3]. Compared with above spectra, some additional absorption bands appear in the spectrum of imprinted ICTX@Mfa without elution, which should be caused by the ciprofloxacin template molecules, where the absorption band at 1621 cm^{-1} results from the group of carbonyl groups (C=O) or carbon-carbon double bonds (C=C) [28], 1600 cm^{-1} to 1450 cm^{-1} are assigned to the stretching vibration of benzene ring, 1400 cm^{-1} belongs to the hydroxyl groups (-OH) or carbon-nitrogen single bonds (C-N), 1300 cm^{-1} is attributed to the stretching vibration of carbon-oxigen single bonds (C-O)[13], 1260cm^{-1} and 1040 cm^{-1} are attributed to the flexural vibration of methylene groups (-CH_2-) or the stretching vibration of carbon-oxigen single bonds (C-O)[28, 50], 1200 cm^{-1} is assigned to the flexural vibration of carbon-nitrogen single bonds (C-N)[8], respectively. All above indicate that ciprofloxacin can easily be embedded in and dislodged from the external $Ti(OH)_4$ xerogel layer, and the target product of imprinted ICTX@Mfa is obtained.

Table 2 Nonmetal contents of Mfa, NICTX@Mfa, ICTX@Mfa with elution and ICTX@Mfa without elution

Samples	C (%)	H (%)	N (%)
Mfa	0	0	0
NICTX@Mfa	3.46	0.48	0.56
ICTX@Mfa with elution	4.33	0.62	0.98
ICTX@Mfa without elution	7.92	1.02	2.47

Furthermore, the nonmetal contents of Mfa, NICTX@Mfa, ICTX@Mfa with elution and ICTX@Mfa without elution samples are detected by an element analyzer. As shown in Table 2. It can be found that, compared with Mfa without containing nonmetal elements, the C (3.46%), H (0.48%) and N (0.56%) contents in the non-imprinted NICTX@Mfa sample are relative low, which results from the organic constituents modified on the surface of Mfa (such as 3-aminopropyltriethoxysilane and succinic anhydride etc.). However, it is worth noting that, before the imprinted ICTX@Mfa sample is eluted, C (7.92%), H (1.02%) and N (2.47%) contents are obviously far higher than that of non-imprinted NICTX@Mfa (C of 3.46%, H of 0.48% and N of 0.56%), implying that the ciprofloxacin template molecules are successfully embedded in the external $Ti(OH)_4$ xerogel layer. In contrast, undergoing elution, the C (4.33%), H (0.62%) and N (0.98%) contents in imprinted ICTX@Mfa sample display the reduction again, which are in close proximity to that of non-imprinted NICTX@Mfa. It indicates that ciprofloxacin template molecules are also easy completely dislodged from the external $Ti(OH)_4$ xerogel layer. These results are well consistent with that obtained from FT-IR spectra.

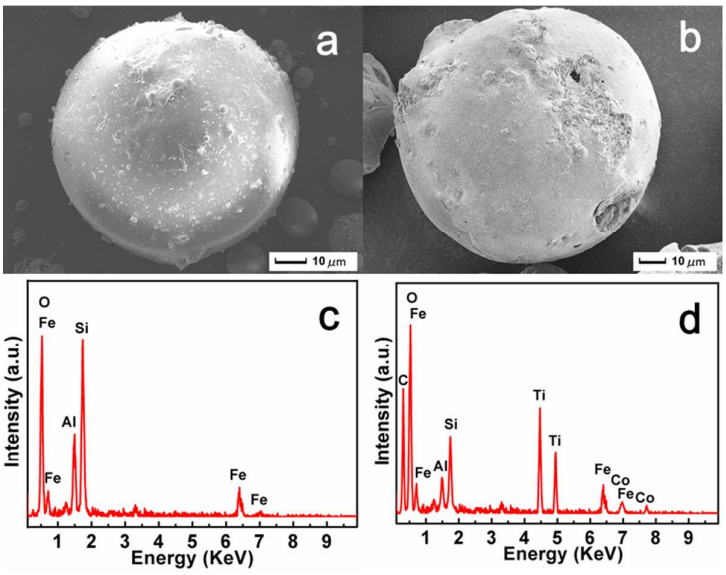

Fig. 4 SEM images and EDS spectra of Mfa (a and c) and ICTX@Mfa (b and d)

The morphologies of Mfa and the target product of imprinted ICTX@Mfa samples are observed by SEM images. As can be seen from Fig. 4a, the original Mfa has a good spherical feature with the average diameter of 80 μm owing to the strict magnet separation. Interestingly, as shown in Fig. 4b, the diameter of ICTX@Mfa with elution reaches to 100 μm, which implies the $Ti(OH)_4$ xerogel layer is efficiently coated on the surface Mfa and has a thickness of ~20 μm. In addition, the clear imprinted layer with lots of imprinted cavities can also be observed on the broken surface of ICTX@Mfa sample, which is a main reason that it has a large specific surface area as following discussions. In addition, EDS spectra in Fig. 4c and Fig. 4d are performed to investigate surface chemical state of the Mfa and ICTX@Mfa. Compared with Mfa, Ti and Co elements are detected besides O, Fe, Al and Si, which agree well with the results of ICP-OES analyses. It indirectly certify the $Ti(OH)_4$ xerogel layer is successfully coated on the surface of Mfa.

Table 3 Specific surface area, pore volume and average pore diameter of different samples

Samples	Specific surface area (m^2 g^{-1})	Pore volume (cm^3 g^{-1})	Pore diameter (nm)
Mfa	5.87	0.01	8.45
NITX@Mfa	20.98	0.07	13.87
NICTX@Mfa	22.35	0.06	11.24
ITX@Mfa	184.15	0.12	2.71
ICTX@Mfa	199.09	0.13	2.55

The specific surface area, pore volume and average pore diameter of Mfa, non-imprinted NITX@Mfa, imprinted ITX@Mfa, non-imprinted NICTX@Mfa, and imprinted ICTX@Mfa are analyzed via nitrogen adsorption-desorption experiments. We notice that the specific surface area, pore volume and average pore diameter of non-imprinted NITX@Mfa and NICTX@Mfa are distinctly larger than that of Mfa, which are mainly due to the coated $Ti(OH)_4$ xerogel layer on the surface of Mfa. In contrast, the specific surface area of imprinted ITX@Mfa and ICTX@Mfa reaches to 184.15 m^2 g^{-1} and 199.09 m^2 g^{-1}, which is 8.8 times and 8.9 times to that of the non-imprinted NITX@Mfa (20.98 m^2 g^{-1}) and NICTX@Mfa (22.35 m^2 g^{-1}), respectively. Meanwhile, the pore volume and average pore diameter of imprinted ITX@Mfa and ICTX@Mfa are obviously larger and smaller than that of the non-imprinted NITX@Mfa and NICTX@Mfa, respectively. These properties may result from the left three-dimensional imprinted cavities after ciprofloxacin template molecules in the $Ti(OH)_4$ xerogel layer is removed out. The above microstructure features are very favor of improving the adsorption property, photocatalytic activity and selectivity.

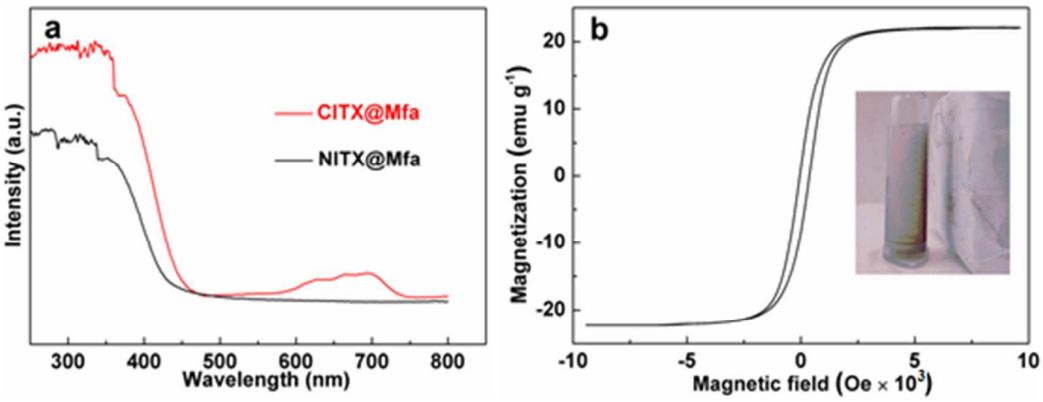

Fig. 5 UV-vis DRS of NITX@Mfa and ICTX@Mfa (a), hysteresis loop of ICTX@Mfa (b) and the photograph of ICTX@Mfa separated from solution using a magnet (inset of b)

UV-vis DRS of non-imprinted NITX@Mfa and imprinted ICTX@Mfa are carried out to research the change of light absorption ability. As can be seen from Fig. 5a, the absorption edge of NITX@Mfa is ~430 nm. However, after doping Co^{2+} ions, the absorption edge increases to ~445 nm and a wide absorption band from 500 nm to 750 nm is produced in the UV-vis DRS of ICTX@Mfa, which greatly enhances the harvest region of visible light. The improvement of light absorption of ICTX@Mfa may be attributed to the generated impurity energy level resulting from Co^{2+} ions, which is one of the important reasons to improve photocatalytic activity. The magnetic property of ICTX@Mfa is investigated by using the VSM system at room temperature to inspect its retrievability. Fig. 5b presents the magnetic hysteresis loop of ICTX@Mfa with a magnetic saturation value of ~22.21 emu g^{-1}, which demonstrates the sample exhibits distinct magnetism. Moreover, the magnetic separation ability of ICTX@Mfa is tested using a magnet. From the photograph (the inset of Fig. 5b), it clearly shows that ICTX@Mfa can be easily separated from the solution by a magnet, which indicates that it possesses good magnetic separation performance.

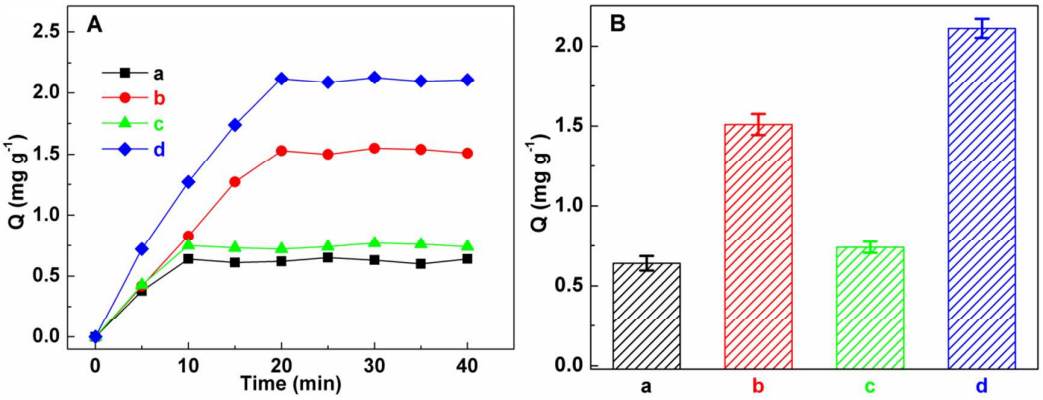

Fig. 6 Adsorption curves of ciprofloxacin over the different samples (A) and the adsorption capacity of different photocatalysts for ciprofloxacin in 40 min in the dark (B) (a: NITX@Mfa, b: ITX@Mfa, c: NICTX@Mfa, d: ICTX@Mfa)

In order to investigate the adsorption capacity and optimal adsorption time of samples, the

adsorption experiments of ciprofloxacin over non-imprinted NITX@Mfa, imprinted ITX@Mfa, non-imprinted NICTX@Mfa and imprinted ICTX@Mfa are performed. As displayed in Fig. 6A, the adsorption capacity of non-imprinted NITX@Mfa and NICTX@Mfa increase significantly before 10 min. After 10 min, the adsorption capacity becomes gentle and steady. In contrast, for imprinted ITX@Mfa and ICTX@Mfa, the adsorption-desorption equilibrium has a longer period of 20 min, which reaches to 2 times to that (10 min) of non-imprinted NITX@Mfa and NICTX@Mfa. It implies that that imprinted samples should have the higher adsorption capacity than non-imprinted samples, just as the results reveled in Fig. 6B. Obviously, the adsorption capacity of imprinted ICTX@Mfa (2.11 mg g^{-1}) and ITX@Mfa (1.51 mg g^{-1}) is much higher than that of non-imprinted NICTX@Mfa (0.74 mg g^{-1}) and NITX@Mfa (0.64 mg g^{-1}), respectively. Such a big difference is attributed to the plenty of three-dimensional imprinted cavities existed in the imprinted $Ti(OH)_4$ xerogel layer that have strong recognition ability for ciprofloxacin molecules. It is desired and reasonable based on the analysis results obtained in nitrogen adsorption-desorption experiments.

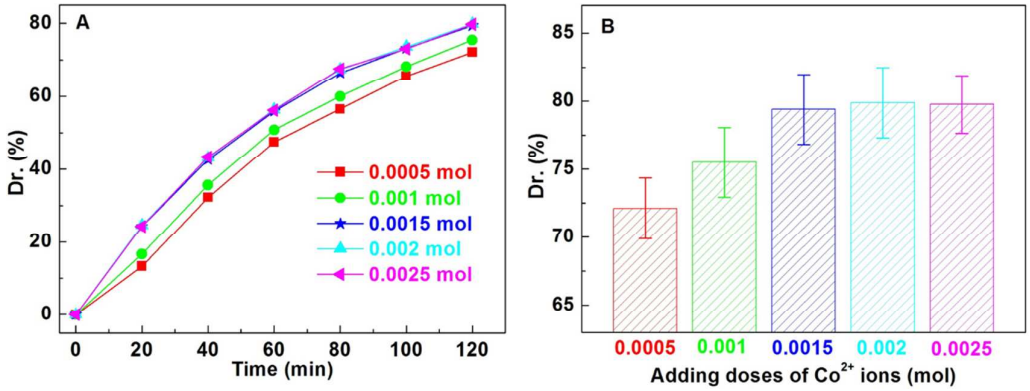

Fig. 7 Influence of different adding doses of Co^{2+} ions on photocatalytic activity of degradation of ciprofloxacin over ICTX@Mfa (A) and the degradation rates of ciprofloxacin over ICTX@Mfa in 120 min under visible light irradiation (B)

In order to achieve better degradation efficiency, the influence of different adding doses of Co^{2+} ions on photocatalytic activity of degradation of ciprofloxacin over ICTX@Mfa is investigated. As shown in Fig. 7, with the increase of the adding dose of Co^{2+} ions, the degradation rate enhances obviously, because the addition of Co^{2+} ions results in the generated impurity energy level which mainly enhances the photocatalytic activity. While when the adding dose is higher than 0.0015 mol, Co^{2+} ions reach saturation, this leads to a very small change in the photocatalytic activity. Taking into account the input costs and photocatalytic performance, 0.0015 mol is the most suitable adding dose of Co^{2+} ions. Therefore, at the following experiments, 0.0015 mol is chosen as the adding dose of Co^{2+} ions to synthesize ICTX@Mfa.

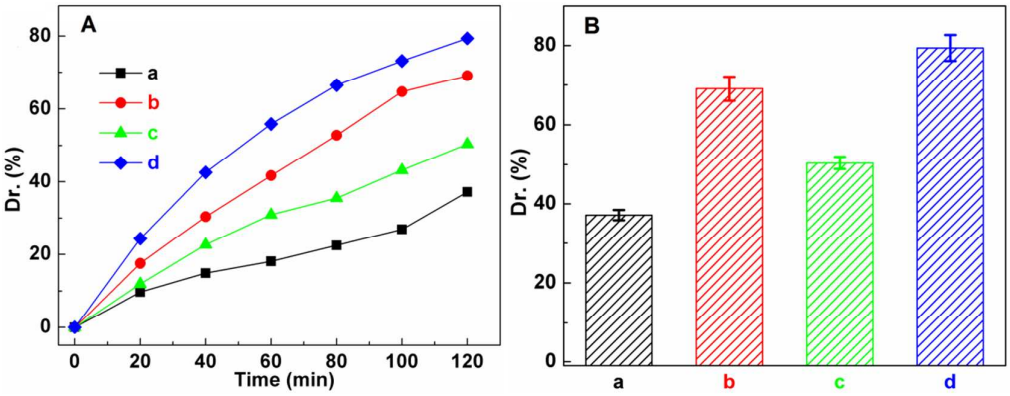

Fig. 8 Degradation curves of ciprofloxacin over the different samples (A) and the degradation rates of ciprofloxacin over the different photocatalysts in 120 min under visible light irradiation (B)

a: NITX@Mfa, b: ITX@Mfa, c: NICTX@Mfa, d: ICTX@Mfa

The photocatalytic activity of different samples is further evaluated by means of degrading ciprofloxacin. Fig. 8A presents the degradation curves of ciprofloxacin over the different samples in the photocatalytic reaction of 120 min, where the photocatalytic activity follows the following order, ICTX@Mfa > ITX@Mfa > NICTX@Mfa > NITX@Mfa. Fig. 8B further shows that the photodegradation rate of imprinted ICTX@Mfa (79.4%) and imprinted ITX@Mfa (69.09 %) is

much higher than that of non-imprinted NICTX@Mfa (50.4 %) and non-imprinted NITX@Mfa (37.17 %), respectively. It is in accordance with law of adsorption, which results from the plenty of three-dimensional imprinted cavities existed in the imprinted $Ti(OH)_4$ xerogel layer that has strong recognition ability for ciprofloxacin molecules. Furthermore, the photodegradation rate of the Co^{2+} doped ICTX@Mfa (79.4%) and NICTX@Mfa (50.4 %) is also higher than that of undoped ITX@Mfa (69.09 %) and NITX@Mfa (37.17 %), respectively, which is mainly due to the fact that two formers have the wider visible light harvest ability. Therefore, the target product of ICTX@Mfa exhibits the superior photocatalytic activity for degrading ciprofloxacin besides its good adsorption property.

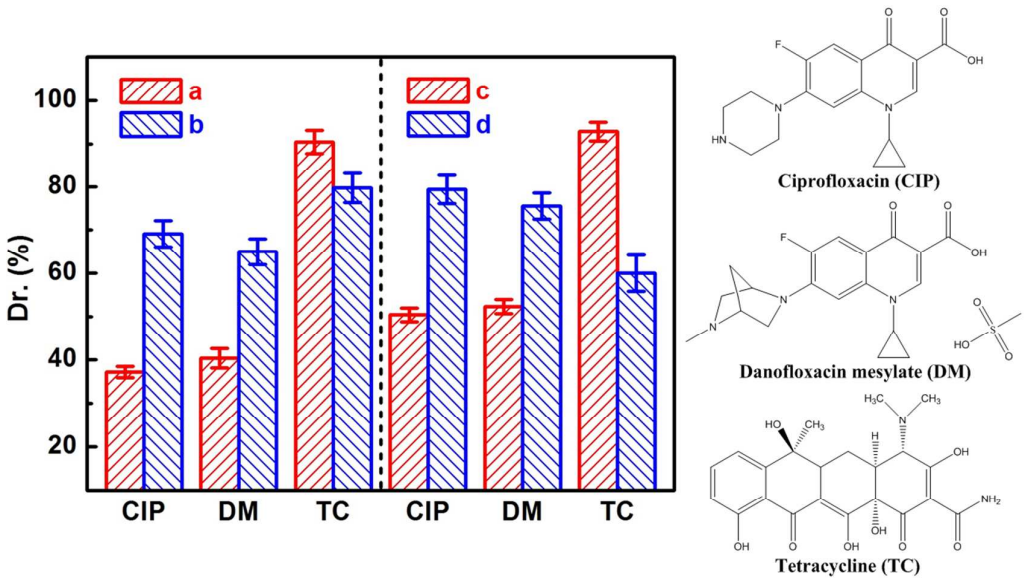

Fig. 9 Contrastive photodegradation rates of ciprofloxacin, danofloxacin mesylate and tetracycline over the different samples in 120 min under the visible light irradiation, a: NITX@Mfa, b: ITX@Mfa, c: NICTX@Mfa, d: ICTX@Mfa

The photodegradation selectivity of the samples is appraised by comparing the degradation rate of ciprofloxacin, danofloxacin mesylate and tetracycline over the imprinted and non-imprinted sample, respectively. As displayed in Fig. 9, the degradation rate of ciprofloxacin

over non-imprinted NITX@Mfa is only 37.17 %, but that over imprinted ITX@Mfa distinctly increases to 69.09 %. In contrast, the degradation rate of tetracycline over non-imprinted NITX@Mfa reaches up to 90.43 %, but that over imprinted ITX@Mfa exhibits abnormally reduction and is only 79.73 %. The similar results take place on the non-imprinted NICTX@Mfa and imprinted ICTX@Mfa. For ciprofloxacin, the degradation rate of 50.4 % over non-imprinted NICTX@Mfa soars up to 79.4 % over imprinted ICTX@Mfa, while the tetracycline degradation rate of 92.82 % over non-imprinted NICTX@Mfa quickly reduces to 50.4 % over imprinted ICTX@Mfa. The reasons for these results are that, ciprofloxacin is used as the template molecule, which can be specifically recognized by the imprinted cavities of ITX@Mfa and ICTX@Mfa. The photodegradation reaction of ciprofloxacin can take place both outside surface and cavity inner. The enlarged specific surface area indicates the effective active sites increase so that the degradation rate of ciprofloxacin also increases sharply. With regard to tetracycline, it has a different molecule structure with ciprofloxacin, resulting in being not recognized. The photodegradation reaction of tetracycline only occurs on the outside surface. The surface imprinted cavities of ciprofloxacin directly result in the effective active sites reduction on the outside surface, thus reducing degradation rate of tetracycline. Besides, due to the fact that the molecule structures of ciprofloxacin and danofloxacin mesylate are very similar, the degradation trend of danofloxacin mesylate over different samples is also similar with that of ciprofloxacin over the corresponding samples, but the degradation rates of danofloxacin mesylate over ITX@Mfa and ICTX@Mfa still reduce compared with those of ciprofloxacin. Thereby, the comparison of degrading ciprofloxacin and danofloxacin mesylate further indicated that the photodegradation selectivity mainly depended on the molecule structure. Owing to the similar

structure, danofloxacin mesylate can be degraded not only on the surface of ICTX@Mfa, but also in some cavity inner occasionally. Therefore, the target product of ICTX@Mfa not only presents the highest photocatalytic activity for removing ciprofloxacin, danofloxacin mesylate and tetracycline, but also possesses the strong specific oriented recognition ability for selectivity degrading ciprofloxacin. We should point out that the photodegradation reaction of tetracycline molecules only take place on the surface of ICTX@Mfa. However, besides surface reaction, ciprofloxacin molecules can easily embed into the imprinted cavities on the surface of ICTX@Mfa and are degraded. Similarly, in addition to the outside surface, the photodegradation reaction of danofloxacin mesylate can also take place in some cavity inner occasionally.

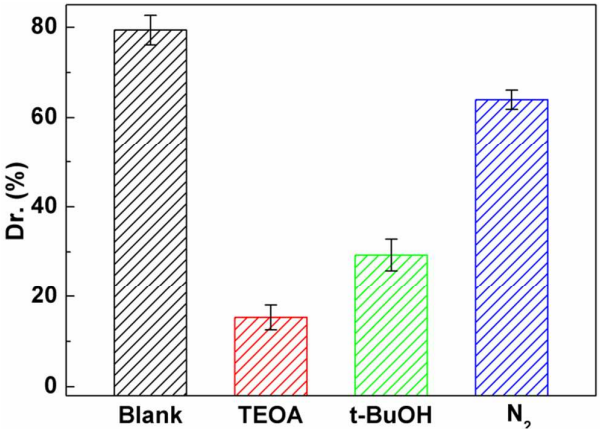

Fig. 10 Degradation rates of ciprofloxacin over ICTX@Mfa in presence of different substrates in 120 min under the visible light irradiation

It is well known that the active species play the important roles in the photodegradation reaction. Consequently, the active species detection experiments are carried out at the degrading ciprofloxacin process over the ICTX@Mfa sample. At the beginning of photocatalytic reaction, triethanolamine (TEOA) or tert-butyl alcohol (t-BuOH) are added into the ciprofloxacin solution serving as h^+ or hydroxyl radical (·OH) capturer, respectively. In addition, nitrogen (N_2) is continuously bubbled into the ciprofloxacin solution to detect superoxide radical ($\cdot O_2^-$) via

inhibiting it's the generation. Fig. 10 shows the resulting degradation rates of ciprofloxacin at the different conditions in 120 min under the visible light irradiation. It can be clearly seen that the addition of TEOA and t-BuOH has significant effect on the photocatalytic activity of ICTX@Mfa because the degradation of ciprofloxacin reduce to 15.3% and 29.3% compared with that of 79.4% without capturer, respectively. In addition, N_2 also has a little effect on the photocatalytic activity of ICTX@Mfa owing to the ciprofloxacin degradation rate of 63.9%. Therefore, h^+ and ·OH are the main oxidative species, and $\cdot O_2^-$ plays only a small role.

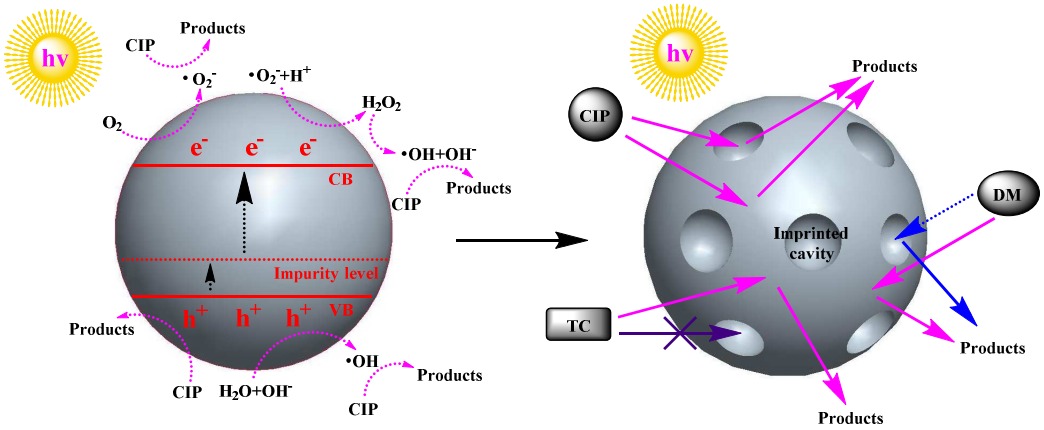

Fig. 11 the possible photocatalytic mechanism over ICTX@Mfa for degrading selectively ciprofloxacin (CIP) by comparing with danofloxacin mesylate (DM) and tetracycline (TC)

Based on the above results, the possible photocatalytic mechanism is proposed, which is shown in Fig. 11. When ICTX@Mfa is exposed to the visible light, the electrons (e^-) on VB are excited into the impurity level and further transfer to CB. The holes (h^+) are also generated on VB simultaneously. Then the photogenerated electrons on CB are captured by dissolved O_2 to produce superoxide radicals ($\cdot O_2^-$), and further produce hydroxyl radicals (·OH). $\cdot O_2^-$ and ·OH originated from O_2 play only a minor role in degrading ciprofloxacin. Meanwhile, the photogenerated holes can directly oxide ciprofloxacin or further oxide H_2O/OH^- to ·OH to degrade ciprofloxacin. The holes and ·OH generated from H_2O/OH^- play a major role in degrading ciprofloxacin. We should

point out that tetracycline molecules only take place photodegradation reaction on the surface of ICTX@Mfa. However, besides surface reaction, ciprofloxacin molecules can easily embed into the imprinted cavities on the surface of ICTX@Mfa and are degraded. Similarly, in addition to the outside surface, the photodegradation reaction of danofloxacin mesylate can also take place in some cavity inner occasionally.

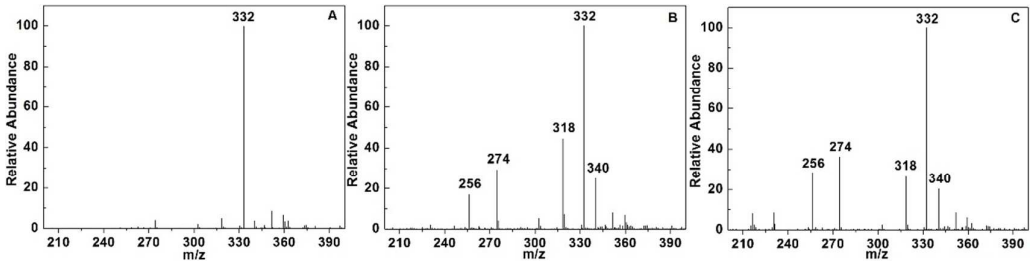

Fig. 12 m/z of degrading ciprofloxacin over ICTX@Mfa (A. the initial ciprofloxacin solution, B. degradation of ciprofloxacin in 60 min, C. degradation of ciprofloxacin in 120 min)

In order to investigate the photodegradation process in depth, HPLC-MS is employed to identify the intermediates, which was shown in Fig. 12. According to the change of the measured mass, the possible intermediate products of photodegradation of ciprofloxacin over ICTX@Mfa are analyzed. As displayed in Fig. 13, ciprofloxacin is fragmented into A ((m/z = 318) by leaving the group of =O and simultaneously becomes B (m/z = 340) owing to the addition reaction, as the reaction proceeded, A ((m/z = 318) is fragmented into C (m/z = 274) by leaving the group of —COOH, afterwards, by leaving the group of —F, C (m/z = 274) is further fragmented into D (m/z = 256), finally, all above intermediate products may be degraded to CO_2, H_2O and other molecules.

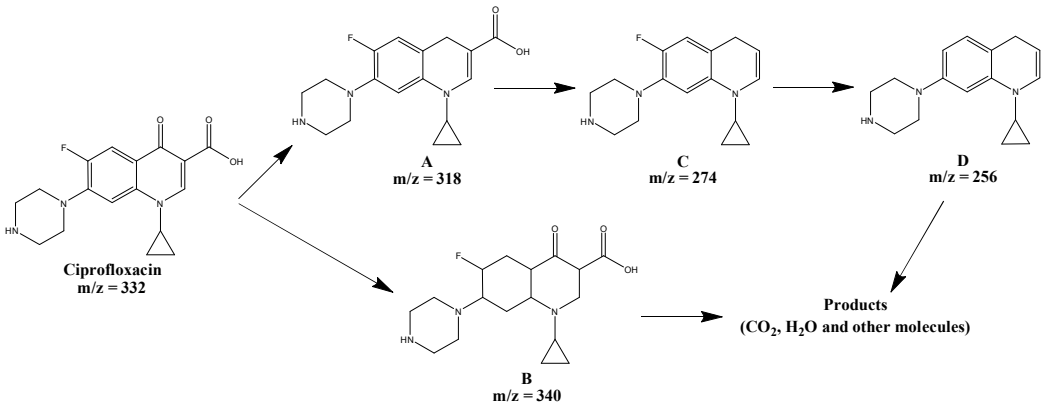

Fig. 13 The possible intermediate products of photodegradation of ciprofloxacin over ICTX@Mfa

Considering that the stability of photocatalyst is very important in the practical application, the circle runs of degrading ciprofloxacin over ICTX@Mfa under the visible light irradiation are carried out. From degradation kinetic curves of ciprofloxacin in Fig. 14, the degradation rate of ciprofloxacin has almost no reduction undergoing 5 cycles, indicating that ICTX@Mfa has the superior stability. In addition, the SEM images of ICTX@Mfa before and after reaction are also performed. We find that the SEM image of the sample after 5 cycles is nearly the same as that of the original sample, which further demonstrates ICTX@Mfa is a stable recyclable photocatalyst.

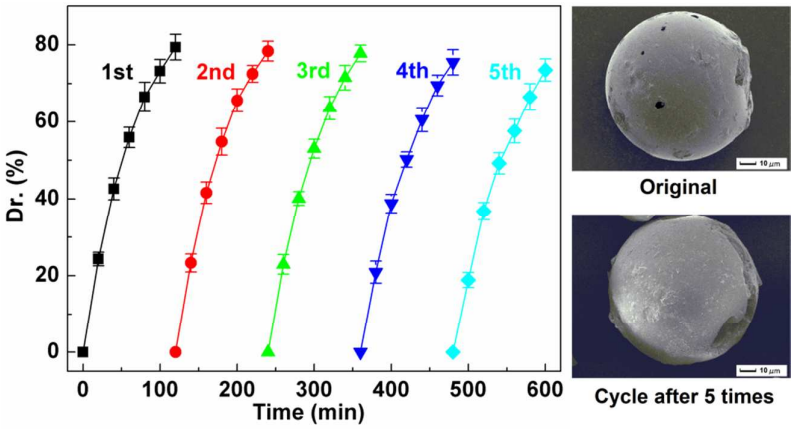

Fig. 14 Degradation rates of ciprofloxacin over ICTX@Mfa in 120 min under the visible light irradiation undergoing 5 cycles and the SEM images of ICTX@Mfa before and after reaction

Conclusions

In summary, a new imprinted photocatalyst ICTX@Mfa with the outstanding stability and retrievability is obtained by means of the molecular imprinting technique, which has the high photodegradation activity for removing common antibiotic ciprofloxacin under the visible light. The as-prepared ICTX@Mfa exhibits a superior specific oriented recognition capability for selectively degrading ciprofloxacin molecules by comparing with danofloxacin mesylate and tetracycline. The photocatalytic reaction mechanism ascertained that the major photoreaction approaches of ciprofloxacin molecules on the surface of ICTX@Mfa arise from the chief contribution of holes and hydroxyl radicals as well as secondary role of superoxide radicals. This work puts forward a new design idea and provides an illustrative example for selectively oriented removing the specified organic pollutant molecules according to the practical requirements.

Acknowledgements

This work was financially supported by the National Natural Science Foundation of China (No. 21306068), the Natural Science Foundation of Jiangsu Province (Nos. BK20130477, BK20130480, BK20130487 and BK20140532), the China Postdoctoral Science Foundation (Nos. 2012M521015 and 2014T70486), the Innovation Programs Foundation of Jiangsu Province (No. CXZZ13_0693) and the University Professional Degree Postgraduate Research Practice Program of Jiangsu Province (No. 1011310016).

References

1 Y. F. Li and Z. P. Liu, *J. Am. Chem. Soc.*, 2011, **133**, 15743.

2 D. Spasiano, R. Marotta, S. Malato, P. Fernandez-Ibañez and I. D. Somma, *Appl. Catal. B*, 2015, **170–171**, 90.

3 H. Dong, G. Chen, J. Sun, C. Li, Y. Yu and D. Chen, *Appl. Catal. B*, 2013, **134–135**, 46.

4 H. Dong, J. Sun, G. Chen, C. Li, Y. Hua and C. Lv, *Phys. Chem. Chem. Phys.*, 2014, **16**, 23915.

5 H. J. Dong, G. Chen, J. X. Sun, Y. J. Feng, C. M. Li and C. D. Lv, *Chem. Commun.*, 2014, **50**, 6596.

6 C. M. Li, G. Chen, J. X. Sun, Y. J. Feng, J. J. Liu and H. J. Dong, *Appl. Catal. B*, 2015, **163**, 415.

7 C. M. Li, G. Chen, J. X. Sun, H. J. Dong, Y. Wang and C. D. Lv, *Appl. Catal. B*, 2014, **160–161**, 383.

8 X. N. Li, J. H. Wang, A. I. Rykov, V. K. Sharma, H. Z. Wei, C. Z. Jin, X. Liu, M. R. Li, S. H. Yu, C. L. Sun and D. D. Dionysiou, *Catal. Sci. Technol.*, 2015, **5**, 504.

9 J. Lee, D. C. Sorescu and X. Y. Deng, *J. Am. Chem. Soc.*, 2011, **133**, 10066.

10 B. Z. Tian, R. F. Dong, J. M. Zhang, S. Y. Bao, F. Yang and J. L. Zhang, *Appl. Catal. B*, 2014, **158**, 76.

11 S. Wang, L. Zhao, L. N. Bai, J. M. Yan, Q. Jiang and J. S. Lian, *J. Mater. Chem. A*, 2014, **2**, 7439.

12 M. V. Sofianou, N. Boukos, T. Vaimakis and C. Trapalis, *Appl. Catal. B*, 2014, **158**, 91.

13 K. Ullah, S. Ye, Z. Lei, K. Y. Cho and W. C. Oh, *Catal. Sci. Technol.*, 2015, **5**, 184.

14 Z. Y. Lu, M. He, L. L. Yang, Z. F. Ma, L. Yang, D. D. Wang, Y. S. Yan, W. D. Shi, Y. Liu and Z. F. Hua, *RSC Adv.*, 2015, **5**, 47820.

15 F. Deng, Y. Liu, X. B. Luo, S. L. Wu, S. L. Luo, C. Au and R. X. Qi, *J. Hazard. Mater.*, 2014,

278, 108.

16 X. T. Shen, L. H. Zhu, N. Wang, T. Zhang and H. Q. Tang, *Catal. Today*, 2014, **225**, 164.

17 L. Ciccotti, L. A. S. do Vale, T. L. R. Hewer and R. S. Freire, *Catal. Sci. Technol.*, 2015, **5**, 1143.

18 Z. Y. Lu, F. Chen, M. He, M. S. Song, Z. F. Ma, W. D. Shi, Y. S. Yan, J. Z. Lan, F. Li and P. Xiao, *Chem. Eng. J.*, 2014, **249**, 15.

19 L. F. Qi, W. Ho, J. L. Wang, P. Y. Zhang and J. G. Yu, *Catal. Sci. Technol.*, 2015, **5**, 2366.

20 Y. Y. Luo, Z. Y. Lu, Y. H. Jiang, D. D. Wang, L. L. Yang, P. W. Huo, Z. L. Da, X. L. Bai, X. L. Xie and P. Y. Yang, *Chem. Eng. J.*, 2014, **240**, 244.

21 W. Chen, W. Lei, M. Xue, F. Xue, Z. H. Meng, W. B. Zhang, F. Qu and K. J. Shea, *J. Mater. Chem. A*, 2014, **2**, 7165.

22 A. Cumbo, B. Lorber, P. F. X. Corvini, W. Meier and P. Shahgaldian, *Nat. Commun.*, 2013, **4**, 1503.

23 Z. Y. Lu, P. W. Huo, Y. Y. Luo, X. L. Liu, D. Wu, X. Gao, C. X. Li and Y. S. Yan, *J. Mol. Catal. A*, 2013, **378**, 91–98.

24 S. D. Pan, H. Y. Shen, L. X. Zhou, X. H. Chen, Y. G. Zhao, M. Q. Cai and M. C. Jin, *J. Mater. Chem. A*, 2014, **2**, 15345.

25 Q. Y. Niu, K. Z. Gao, Z. H. Lin and W. H. Wu, *Chem. Commun.*, 2013, **49**, 9137.

26 Y. G. Zhao, X. H. Chen, S. D. Pan, H. Zhu, H. Y. Shen and M. C. Jin, *J. Mater. Chem. A*, 2013, **1**, 11648.

27 S. S. Wang, J. Ye, Z. J. Bie and Z. Liu, *Chem. Sci.*, 2014, **5**, 1135.

28 Z. Y. Lu, Y. Y. Luo, M. He, P. W. Huo, T. T. Chen, W. D. Shi, Y. S. Yan, J. M. Pan, Z. F. Ma and

S. Y. Yang, *RSC Adv.*, 2013, **3**, 18373.

29 F. Deng, Y. X. Li, X. B. Luo, L. X. Yang and X. M. Tu, *Colloid. Surf. A*, 2012, **395**, 183.

30 M. A. Niedermeier, I. Groß and P. Müller-Buschbaum, *J. Mater. Chem. A*, 2013, **1**, 13399.

31 S. T. Wei, X. L. Hu, H. L. Liu, Q. Wang and C. Y. He, *J. Hazard. Mater.*, 2015, **294**, 168.

32 M. A. Niedermeier, G. Tainter, B. Weiler, P. Lugli and P. Müller-Buschbaum, *J. Mater. Chem. A*, 2013, **1**, 7870.

33 P. W. Huo, Z. Y. Lu, X. L. Liu, D. Wu, X. L. Liu, J. M. Pan, X. Gao, W. L. Guo, H. M. Li and Y. S. Yan, *Chem. Eng. J.*, 2012, **189–190**, 75.

34 F. Deng, K. Li, X. B. Luo, S. L. Luo, G. S. Zeng, S. L. Wu and C. Au, *Sci. Adv. Mater.*, 2014, **6**, 577.

35 X .L. Liu, P. Lv, G. X. Yao, C. C. Ma, P. W. Huo and Y. S. Yan, *Chem. Eng. J.*, 2013, **217**, 398.

36 X. B. Luo, F. Deng, L. J. Min, S. L. Luo, B. Guo, G. S. Zeng and C. Au, *Environ. Sci. Technol.*, 2013, **47**, 7404.

37 C. X. Huang, Z. K. Tu and X. T. Shen, *J. Hazard. Mater.*, 2013, **248–249**, 379.

38 J. B. M. Goodall, D. Illsley, R. Lines, N. M. Makwana and J. A. Darr, *ACS Comb. Sci.*, 2015, **17**, 100.

39 T. Wang, X. G. Meng, G. G. Liu, K. Chang, P. Li, Q. Kang, L. Q. Liu, M. Li, S. X. Ouyang and J. H. Ye, *J. Mater. Chem. A*, 2015, **3**, 9491.

40 S. Kuriakose, B. Satpati and S. Mohapatra, *Phys. Chem. Chem. Phys.*, 2014, **16**, 12741.

41 H. Li, B Xu, F. Qi, D. Sun and Z. Chen, *Appl. Catal. B*, 2014, **152–153**, 342.

42 Z. Y. Lu, W. C. Zhou, P. W. Huo, Y. Y. Luo, M. He, J. M. Pan, C. X. Li and Y. S. Yan, *Chem. Eng. J.*, 2013, **225**, 34.

43 P. W. Huo, Z. Y. Lu, H. Q. Wang, J. M. Pan, H. M. Li, X. Y. Wu, W. H. Huang and Y. S. Yan, *Chem. Eng. J.*, 2011, **172**, 615.

44 J. M. Pan, W. Hu, X. H. Dai, W. Guan, X. H. Zou, X. Wang, P. W. Huo and Y. S. Yan, *J. Mater. Chem.*, 2011, **21**, 15741.

45 X. N. Yu, X. Gao, Z. Y. Lu, X. L. Liu, P. W. Huo, X. L. Liu, D. Wu and Y. S. Yan, *RSC Adv.*, 2013, **3**, 14807.

46 M. He, Z. Y. Lu, W. C. Zhou, T. T. Chen, W. D. Shi, G. B. Che, P. W. Huo, Z. Zhu, X. X. Zhao and Y. S. Yan, *RSC Adv.*, 2014, **4**, 60148.

47 J. M. Pan, H. Yao, X. X. Li, B. Wang, P. W. Huo, W. Z. Xu, H. X. Ou and Y. S. Yan, *J. Hazard. Mater.*, 2011, **190**, 276.

48 Z. L. Shi, S. H. Yao and C. C. Sui, *Catal. Sci. Technol.*, 2011, **1**, 817.

49 H. Dang, X. Dong, Y. Dong, H. Fan and Y. Qiu, *Mater. Lett.*, 2015, **138**, 56.

50 P. W. Huo, Z. Y. Lu, X. L. Liu, X. L. Liu, X. Gao, J. M. Pan, D. Wu, J. Ying, H. M. Li and Y. S. Yan, *Chem. Eng. J.*, 2012, **198–199**, 73.

Gpaphical abstract

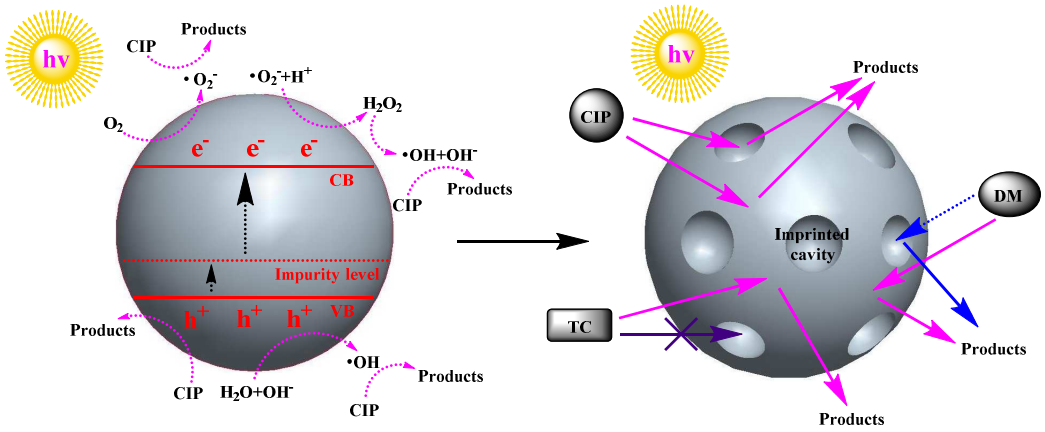

A new imprinted photocatalyst ICTX@Mfa is prepared, which exhibits the superior specific oriented recognition capability, stability and retrievability for selectively degrading ciprofloxacin under the visible light. Degradation approaches of ciprofloxacin arise from the chief contribution of holes and hydroxyl radicals as well as secondary role of superoxide radicals.